approximation, and even with anharmonicities, they are expected to be very small.

15. R. B. Gerber and M. A. Ratner, *Adv. Chem. Phys.* **70**, 97 (1988).
16. M. A. Ratner and R. B. Gerber, *J. Phys. Chem.* **90**, 20 (1986).
17. T. R. Horn, R. B. Gerber, M. A. Ratner, *J. Chem. Phys.* **91**, 1813 (1989).
18. H. Romanowski, J. M. Bowman, L. Harding, *ibid.* **82**, 4155 (1985).
19. All calculations were conducted on a Convex c240 computer. The normal modes were computed with a library parallel routine for the matrix diagonalization, a procedure that took 4 hours of computer (CPU) time. The generation of the third- and fourth-derivative matrix elements in normal coordinates was completed in 7 CPU hours. The SCF procedure was the fastest step, taking 19 s per iteration. The solutions to Eq. 3 were performed with a second-order finite-differences algorithm on an equispaced grid.
20. D. J. Nesbitt, *Annu. Rev. Phys. Chem.* **45**, 367 (1994); J. Laane, *ibid.*, p. 179.
21. W. Qian and S. Krimm, *Biopolymers* **34**, 1377 (1994).
22. We are grateful to the Chemistry Division of the National Science Foundation for partial support of this research. R.E. is an Allon Fellow in Israel and wishes to thank the Israel Science Foundation for support. The Fritz Haber Research Center is supported by the Minerva Gesellschaft für die Forschung, München, Germany. R.B.G. thanks the office of academic computing at the University of California at Irvine for the allocation of computational time on the Convex c240.

15 December 1994; accepted 13 March 1995

Pressure-Tuned Fermi Resonance in Ice VII

K. Aoki,* H. Yamawaki, M. Sakashita

Fermi resonance was observed between the OH stretch and the overtone of the OH bending modes of HDO molecules contaminated in phase VII of D_2O ice over the pressure range from 17 to 30 gigapascals. An anharmonic coupling constant, which is related to the potential energy surface on which hydrogen-bonded protons oscillate, was found to range around 50 wave numbers through the resonant pressure range. Its experimentally obtained magnitude and pressure-insensitive behavior will be useful for theoretical studies of the potential energy surface and hence of the nature of hydrogen bonding in ice.

Ice is a prototypical hydrogen-bonded system, and its structural and physical properties have been a major subject of high-pressure research. More than 10 crystalline phases have been found in a pressure range up to 50 GPa and in a temperature range down to 77 K (*1*). Of the known phases, ice VII and VIII are particularly important for understanding the nature of the hydrogen bond. They have very closely related structures (*2–4*) and are stable from 2 GPa to at least 50 GPa (*5*). This wide range of pressure stability allows intermolecular distances to vary widely without any fundamental change in the molecular arrangement. Raman scattering (*5–7*), infrared absorption (*8*), and x-ray diffraction measurements (*9*, *10*) have been used to investigate the high-pressure vibrational and structural behavior of these phases.

Recently, fundamental aspects of the nature of bonding in ice VII and VIII were revealed by high-pressure experiments. The pressure dependence of the hydrogen bond length in ice VIII was directly measured by neutron powder diffraction (*11*), and the elastic property of ice VII was precisely investigated by single crystal Brillouin spectroscopy (*12*). From these experimental results, the pressure dependence of the interatomic potential and the intermolecular bond strength were derived. One interesting feature previously unseen in ice is resonance between the vibrational states associated with the hydrogen bonding. Such a vibrational resonance is known as Fermi resonance and is often observed in complex molecules.

Fermi resonance occurs when two vibrational modes having the same symmetry and comparable vibrational frequencies are coupled by an anharmonic term in the interatomic potential. The coupling of these two vibrational modes produces two stationary resonant states; the frequency splitting and the amplitude distribution between them are described as a function of both an anharmonic coupling constant and the frequency difference between the uncoupled initial states. Such a resonant effect was first observed in the Raman spectra of CO_2 in 1929 (*13*) and a quantum mechanical explanation was immediately given by Fermi (*14*). In solid CO_2, the symmetric stretch and the overtone of the bending modes are coupled to form two stationary resonant states separated by 100 cm^{-1}. The corresponding vibrational modes of H_2O are far from resonance: In the infrared absorption spectra of ice VII at 2 GPa, for instance, the peaks from the stretch and the overtone of the bending modes are at about 3400 and 2900 cm^{-1}, respectively. However, the OH stretching frequency rapidly approaches the overtone frequency with increasing pressure (*8*). The decrease rate, about -20 cm^{-1} per gigapascal, leads to an expectation that the resonance will be induced in ice VII, as it is in solid CO_2, at a pressure of several tens of gigapascals. Here we describe infrared absorption measurements of ice VII up to 45 GPa at room temperature, which demonstrate the presence of pressure-tuned Fermi resonance.

Infrared spectra of HDO molecules contaminated in 99.996% D_2O (Aldrich) were measured in a cylindrical diamond-anvil cell 30 mm in diameter and 20 mm thick, with an optical opening of 60° for both entrance and exit sides (*15*). The sample was sealed in a hole about 80 μm in diameter prepared in a 40-μm-thick metal gasket of Inconel X-750 and squeezed between opposed anvils. The pressure was determined from the shift of the fluorescence lines from ruby chips embedded in the sample (*16*). The pressure difference inside the sample was relatively small; at an average pressure of 36.4 GPa, for example, the measured pressures ranged from 36.3 to 36.5 GPa. Light transmitted through the unmasked sample area, a square typically 60 μm by 60 μm, was analyzed and recorded with a microscope–Fourier transform infrared spectrometer. The spectral resolution was 1.0 cm^{-1}.

The absorption peaks of the stretching and bending vibrations in the HDO molecule were measured at pressures from 2 to 45 GPa. Over this pressure range, ice VII is known to exist stably. For ice VII, prepared just above the transition pressure of 2 GPa, a strong stretching peak was observed at about 3400 cm^{-1} on the tail of the saturated OD stretching peaks, whereas an absorption peak associated with the overtone of the bending vibration was not observed in the expected frequency region around 3000 cm^{-1}. The stretching peak rapidly shifted to a lower frequency with increasing pressure, reaching 3100 cm^{-1} at 15 GPa. The overtone peak of the bending mode was then recognized as a shoulder located at about 2900 cm^{-1}. When the pressure increased further, the two peaks approached closely enough to begin to interfere and showed anomalous changes in frequencies and peak intensities.

Figure 1 shows absorption spectra of the coupled states of the stretch and bending modes in the pressure range from 18 to 27 GPa. The intensities of the two peaks change in the opposite directions as pressure increases. The shoulder peak, initially located at 2900 cm^{-1}, grows gradually, while the height of the large peak at 3100 cm^{-1} decreases. Their peak heights are comparable at 22.9 GPa and then reverse at higher pressures. Finally, the original large peak is depressed to a shoulder at 26.7 GPa. These two peaks are associated with the resonant states formed by the mixing of the stretch and the overtone of the bending modes. The anom-

---

National Institute of Materials and Chemical Research, Tsukuba, Ibaraki 305, Japan.

*To whom correspondence should be addressed.

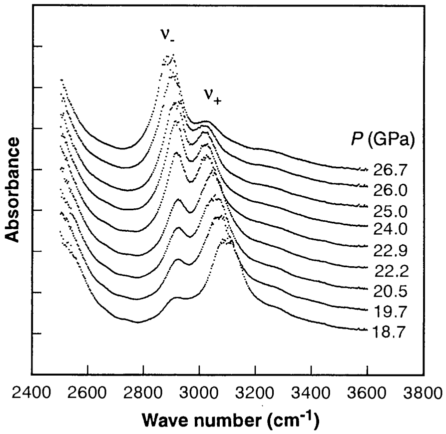

Fig. 1. Infrared absorption peaks of the OH stretching and the overtone of the OH bending vibrations of the HDO molecule in phase VII of D_2O. The numerical values attached to each spectrum indicate the measuring pressures. The mixing of the two vibrational states by Fermi resonance can be seen as a successive change in absorption intensity with increasing pressure.

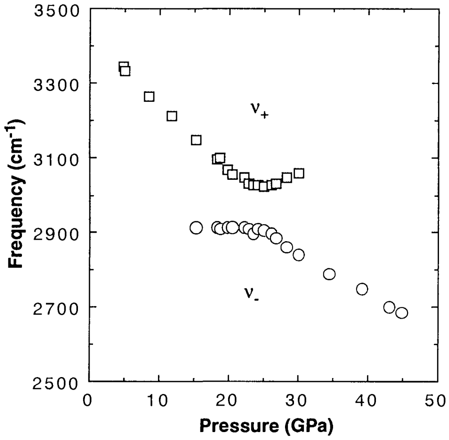

Fig. 2. Variation of the OH stretching frequency ν_+ and the overtone of the OH bending frequency ν_- with pressure. Interference between the two frequencies occurs in the resonant pressure region from 20 to 30 GPa. In the preresonant region below 20 GPa, ν_+ is considered to be the unperturbed stretching frequency, whereas ν_- corresponds to the stretching frequency in the postresonant region above 30 GPa.

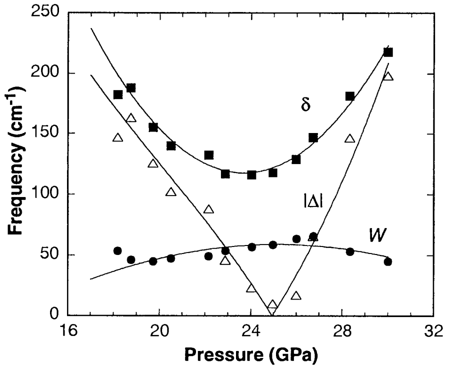

Fig. 3. The pressure dependence of the Fermi resonance parameters for ice VII: the observed, $\delta = \nu_+ - \nu_-$, and unperturbed, $\Delta = \nu_s - 2\nu_b$, separations of the vibrational frequencies and the anharmonic coupling constant W. Solid lines are guides for the eye.

alous change in absorption intensity is interpreted in terms of the pressure variation of the mixing rate of the two unperturbed vibrational modes. The absorption intensity successively moves from the high-frequency to the low-frequency peak while their separation remains nearly constant. Peak overlapping does not occur. This behavior is typical of Fermi resonance.

A perturbation theory is often used for phenomenological analysis of Fermi resonance (*17*). The unperturbed vibrational frequencies, in this case the stretch and the bending modes of OH, are denoted by ν_s and ν_b, respectively. When ν_s and $2\nu_b$ become comparable, the vibrational motions mix through an anharmonic interaction. An anharmonic coupling constant W connects the separation between the observed frequencies, $\delta = \nu_+ - \nu_-$, and that between the unperturbed frequencies, $\Delta = \nu_s - 2\nu_b$, according to

$$\delta^2 = \Delta^2(1 + 4W^2/\Delta^2) \qquad (1)$$

The intensity ratio of the coupled modes is described by

$$R = I_+/I_- = (\delta + \Delta)/(\delta - \Delta) \qquad (2)$$

where the intensity ratio is assumed to be zero for the unperturbed states. The quantities W and Δ can then be derived from the observed vibrational frequencies and peak intensities.

Figure 2 shows the variation of the ν_+ and ν_- frequencies of the coupled states with pressure. We obtained the peak frequencies, as well as the integrated absorption intensities, by fitting the observed spectra with Lorentzian functions. Below 15 GPa, the ν_+ frequency decreases at a rate of -20 cm^{-1} per gigapascal, in agreement with previous results (*8*). Remarkable resonant behavior can be seen in the pressure range between 20 and 30 GPa. At about 25 GPa, the ν_+ frequency reaches a minimum and then increases, whereas the pressure-insensitive ν_- frequency begins to decrease. The two frequencies do not cross, as they should in the absence of Fermi resonance. It is apparent, however, from the intensity change that the character of the vibrational mode alters completely through the resonance: Below 15 GPa, the ν_+ peak can be considered as the OH stretch, whereas above 30 GPa, the ν_- peak corresponds to the OH stretch.

A logarithmic plot of the intensity ratio in the resonant pressure region gives

$$\log (I_+/I_-) = 5.0 - 0.20P \qquad (3)$$

where I is the integrated peak intensity and P is pressure in gigapascals. The pressure coefficient indicates that the intensity ratio decreases by two orders of magnitude for a pressure increase of 10 GPa. An intensity change of this magnitude can be seen in the successively measured spectra in the pressure range from 18 to 27 GPa (Fig. 1).

The calculated values of W and Δ are plotted as a function of pressure in Fig. 3, along with the observed peak separation δ. The resonance is exact at about 25 GPa, where Δ is zero and δ reaches a minimum value of 116 cm^{-1}. Unlike the other parameters, W is pressure-insensitive, ranging over 50 cm^{-1} through the pressure range. The magnitude of resonance can be described by W^2/Δ^2 (Eq. 1). For almost constant W, the resonance is maximized at $\Delta = 0$, where δ becomes equal to $2W$. The deviation between δ and Δ decreases rapidly when the pressure is increased or decreased from the resonant pressure of 25 GPa. Thus, an off-resonant process is attributed to a substantial increase in the separation of the unperturbed vibrational frequencies Δ and not to change in W. Although the shape of the interatomic potential is significantly influenced by pressure, as seen in the large decrease of the stretching frequency, the change in the anharmonic coupling term is small.

At the resonant pressure of 25 GPa, ice VII has a body-centered-cubic lattice of oxygen atoms with some disorder in the positions of the protons (*2, 3*). The principal structural variables describing the hydrogen bond are the distance between the oxygen atoms R_{OO} and the O–H(D) bond length $r_{OH(D)}$. At 2.6 GPa and 293 K, the observed R_{OO} in phase VII of D_2O is 0.2901 nm; r_{OD} is 0.0943 or 0.0959 nm, depending on the model structure adopted (*3*). The distance R_{OO} falls to 0.2564 nm at 25 GPa (*9*). To our knowledge, no high-pressure data are available for the O–H(D) bond length. However, the very close structural relation between ice VII and VIII (*2–4*) and the negligibly small pressure dependence of r_{OD} observed for ice VII (*11*) allow an assumption that the O–H bond length in ice VII should also not change significantly with pressure. Thus, we estimate r_{OH} at 25 GPa to be 0.0951 nm, an average of the two values at 2.6 GPa. The observed Fermi resonance between the stretch and the overtone of the bending modes can be described in terms of these structural variables; the resonance has a tuning point at a pressure where the ratio r_{OH}/R_{OO} increases to 0.371 owing to a unilateral decrease in R_{OO}.

The anharmonic constant observed for ice VII can be compared with that reported for CO_2, the best known molecule showing Fermi resonance. Solid CO_2 has a cubic unit cell containing four molecules with carbon atoms located on the face-centered positions. The molecular axes point in the body-diagonal directions as a result of strong quadrupole-quadrupole interactions between the molecules (*18*). Raman and infrared measurements have revealed that the symmetric stretch and the overtone of the bending vibrational states are located in a postresonant region at atmospheric pressure (*19*, *20*). Hence, application of pressure pushes the partly coupled vibrational states further off-resonance. An exact resonance is predicted to occur at a virtual negative pressure of about -5 GPa, where roughly estimated values of 50 and 105 cm^{-1} were obtained for W and δ, respectively. These values are very close to those of ice VII obtained in the present experiment. This agreement seems to be coincidental, rather than a common tendency in triatomic molecules. The chemical bonds of H_2O and CO_2 are too different to permit the extraction of a general tendency for Fermi resonance in molecular solids.

REFERENCES AND NOTES

1. For instance, see R. J. Hemley, L. C. Chen, H. K. Mao, *Nature* **338**, 638 (1989).
2. W. F. Kuhs, J. L. Finney, C. Vettier, D. V. Bliss, *J. Chem. Phys.* **81**, 3612 (1984).
3. J. D. Jorgensen and T. G. Worlton, *ibid.* **83**, 329 (1985).
4. J. D. Jorgensen *et al.*, *ibid.* **81**, 3211 (1984).
5. Ph. Pruzan *et al.*, *ibid.* **97**, 718 (1992).
6. G. E. Walrafen *et al.*, *ibid.* **77**, 2166 (1982).
7. K. R. Hirsch and W. B. Holzapfel, *ibid.* **84**, 2771 (1986).
8. D. D. Klug and E. Whalley, *ibid.* **81**, 1220 (1984).
9. R. G. Munro, S. Block, F. A. Mauer, G. Piermarini, *J. Appl. Phys.* **53**, 6174 (1982). They used the earlier linear ruby-pressure scale in their x-ray diffraction measurement, which tends to underestimate the pressure, for instance, by 1 GPa at 25 GPa. We have corrected their pressures using the nonlinear ruby-pressure scale given in (*16*).
10. R. J. Hemley *et al.*, *Nature* **330**, 737 (1987).
11. R. J. Nelmes *et al.*, *Phys. Rev. Lett.* **71**, 1192 (1993).
12. H. Shimizu, M. Ohnishi, S. Sasaki, Y. Ishibashi, *ibid.* **74**, 2820 (1995).
13. F. Rasetti, *Nature* **123**, 205 (1929).
14. E. Fermi, *Z. Phys.* **71**, 250 (1931).
15. K. Aoki *et al.*, *Jpn. J. Appl. Phys.* **26**, 2107 (1987).
16. H. K. Mao *et al.*, *J. Appl. Phys.* **49**, 3276 (1978).
17. W. Schindler, T. W. Zerda, J. Jonas, *J. Chem. Phys.* **81**, 4306 (1984).
18. W. H. Keesom and J. W. L. Kohler, *Physica* **1**, 167 (1934).
19. R. C. Hanson and L. H. Jones, *J. Chem. Phys.* **75**, 102 (1981).
20. H. Olijnyk *et al.*, *ibid.* **88**, 4204 (1988).

22 September 1994; accepted 8 March 1995

Mesostructure Design with Gemini Surfactants: Supercage Formation in a Three-Dimensional Hexagonal Array

Qisheng Huo, Rosa Leon, Pierre M. Petroff, Galen D. Stucky*

At low temperatures, liquid crystal–like arrays made up of inorganic-cluster and organic molecular units readily undergo reversible lyotropic transformations. Gemini surfactants, with two quaternary ammonium head groups separated by a methylene chain of variable length and with each head group attached to a hydrophobic tail, can be used to control organic charge sitting relative to the bivariable hydrophobic tail configurations. This approach has led to the synthesis of a mesophase (SBA-2) that has three-dimensional hexagonal ($P6_3/mmc$) symmetry, regular supercages that can be dimensionally tailored, and a large inner surface area. This mesostructure analog of a zeolite cage structure does not appear to have a lyotropic surfactant or lipid liquid crystal mesophase counterpart. Through the modification of gemini charge separation and each of the two organic tails, these syntheses can be used to optimize templating effects, including the synthesis of MCM-48 at room temperature.

Ordered silicate mesoporous molecular sieves have been synthesized (*1*– *5*) by the organization of organic molecules with inorganic molecular species. Low-temperature synthesis methods and kinetic control can be used to uncouple inorganic polymerization from the initial cooperative assembly of inorganic cluster ions and surfactant ions into liquid crystal–like arrays (*4*–*6*). These liquid crystal–like phases are similar to conventional surfactant and lipid lyotropic liquid crystal arrays. However, they cannot be adequately described by thermodynamic and modeling descriptions that only implicitly include polycharged cluster anions as part of the charged bilayer. The multidentate anions have large formation constants with the surfactant cations, have low solubilities, and structurally direct the arrangement of the organic surfactants through both the number of anionic sites that are present (generally determined by pH) and the orientation of the organic surfactant with respect to the molecular inorganic surface (*7*). These characteristics strongly suggest that new lyotropic liquid crystal phases and behavior might be obtained in biphase inorganic-organic mesostructure synthesis. Because of the saltlike character of the product phases and the ability to polymerize the inorganic or organic phase into periodic long-range structures, the mesocomposite materials can be used to study lyotropic liquid crystal–like arrangements in more detail (*6*).

The relative positions and distances of head groups of conventional mono(quaternary ammonium) surfactants are determined mainly by electrostatic interactions, and also by the packing requirements of the disordered alkyl chains. By coupling the head groups with a molecular spacer, one can control the distance between the head groups, that is, the value of a_0, the effective head group area (*8*). Oligomeric or polymeric charged surfactants with a spatially separated charge center can either act as a chelating group to a given cluster surface or serve to orient clusters with respect to each other. By this means, we can change the packing parameter g (*8*) of the surfactant–inorganic cluster unit with polycharged surfactants. In this report, we describe recent mesoporous material synthesis results obtained with gemini surfactants (*9*), $C_nH_{2n+1}N^+(CH_3)_2(CH_2)_sN^+(CH_3)_2$-$C_mH_{2m+1}$ (designated as $C_{n\text{-}s\text{-}m}$), and silica. The mesoporous structure can be considerably modified by changing the length and nature of both the side chain and the spacer group. The end member of this family, $C_{n\text{-}s\text{-}1}$, gives a particularly interesting three-dimensional (3D) hexagonal cage structure (SBA-2). Cage-structured mesoporous solids have possible advantages in catalysis and separation applications. Of the reported mesoporous structures, the M41S molecular sieves, MCM-41 and MCM-48, possess uniform pore channels without cages. The same is true of SBA-3 (acid, pH < 1, synthesized silica phase with an x-ray diffraction pattern similar to that of MCM-41) and cubic phases synthesized in concentrated acid solution (*4*, *5*). For example, the cubic ($Pm\bar{3}n$) silica structure, SBA-1, is synthesized in the presence of surfactants with large head groups (such as, alkyltriethylammonium) in acidic media (*4*). A sample of SBA-1 [cell parameter $a = 79.2$ Å, synthesized with $C_{18}H_{37}N(C_2H_5)_3{}^+$] has a BET (Brunauer-Emmett-Teller) surface area of 1256 m^2 g^{-1}, with a pore diameter of 20

Q. Huo, Department of Chemistry, University of California, Santa Barbara, CA 93106, USA.
R. Leon and P. M. Petroff, QUEST, University of California, Santa Barbara, CA 93106, USA.
G. D. Stucky, Departments of Chemistry and Materials, University of California, Santa Barbara, CA 93106, USA.

*To whom correspondence should be addressed.